

PAGen: Phase-guided Amplitude Generation for Domain-adaptive Object Detection

Shuchen Du Shuo Lei Feiran Li Jiacheng Li Daisuke Iso
Sony Research

{shuchen.du, shuo.lei, feiran.li, jiacheng.li, daisuke.iso}@sony.com

Abstract

Unsupervised domain adaptation (UDA) greatly facilitates the deployment of neural networks across diverse environments. However, most state-of-the-art approaches are overly complex, relying on challenging adversarial training strategies, or on elaborate architectural designs with auxiliary models for feature distillation and pseudo-label generation. In this work, we present a simple yet effective UDA method that learns to adapt image styles in the frequency domain to reduce the discrepancy between source and target domains. The proposed approach introduces only a lightweight pre-processing module during training and entirely discards it at inference time, thus incurring no additional computational overhead. We validate our method on domain-adaptive object detection (DAOD) tasks, where ground-truth annotations are easily accessible in source domains (e.g., normal-weather or synthetic conditions) but challenging to obtain in target domains (e.g., adverse weather or low-light scenes). Extensive experiments demonstrate that our method achieves substantial performance gains on multiple benchmarks, highlighting its practicality and effectiveness.

1. Introduction

Object detection is widely applied in real-world scenarios such as surveillance, autonomous driving, and robotics. Despite its success, training robust detectors for every new environment remains challenging, as collecting high-quality bounding box annotations for each scenario is both costly and labor-intensive. Unsupervised domain adaptation (UDA) addresses this challenge by transferring knowledge from a labeled source domain to an unlabeled target domain, thereby reducing the annotation burden while improving generalization across diverse domains.

Pioneering works on domain-adaptive object detection (DAOD) employ adversarial losses [5, 9, 21, 45, 49, 52, 60] or graph matching [33–35, 39, 40, 58] for domain alignment. However, these methods often bias the detector toward the

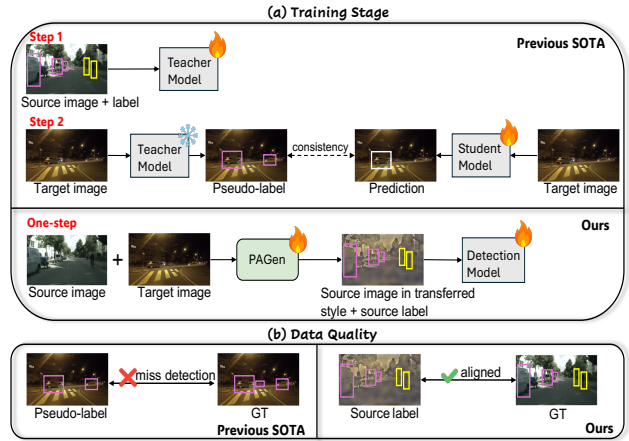


Figure 1. (a) Recent state-of-the-art approaches mainly rely on self-training strategies to generate pseudo labels for target-domain images. Their training procedures are typically complex, often requiring multi-stage optimization and careful balancing among multiple loss terms. In contrast, our method enables a simple end-to-end one-step training pipeline, which greatly facilitates practical deployment. (b) In terms of target-domain data quality, existing methods heavily rely on pseudo labels for consistency training, which can introduce noise due to missed detections. Our approach, however, ensures accurate target supervision without such noise, thus reducing misleading gradients during adaptation.

source domain, as only source-domain images are labeled during training, limiting their effectiveness. As a solution, recent approaches adopt the self-training strategy to generate pseudo labels for the target domain [4, 8, 12, 14, 27, 28, 36], implemented either via a mean-teacher framework [12, 50] or using vision foundation models (VFM) [29, 30, 32]. Although these methods have progressively improved performance, their implementation procedures are often complicated (e.g., requiring careful balancing of multiple losses in a multi-task setting) or resource-intensive (e.g., multi-stage training including large auxiliary models, or VFM with copyright restrictions), limiting their practicality.

We aim to develop a simple yet effective approach for

DAOD. To minimize additional computational overhead and reduce dependency on auxiliary networks as mentioned above, we tackle the problem at the input level. Specifically, we draw inspiration from frequency-domain image decomposition [16]: In the frequency domain, the discrete Fourier transform (DFT) represents an image with its phase and amplitude components, where the phase encodes content and structural layout on which the human perception relies more for semantic recognition, and the amplitude reflects the style and noise that are more domain-sensitive [6, 53]. Based on this property, re-pairing the phase and amplitude components from different images enables the recomposition of content and style, improving model robustness against amplitude variations in different domains.

To this end, we introduce Phase-guided Amplitude Generation (PAGen), a lightweight (only 120k parameters) learnable module that performs input-level style adaptation for the DAOD task. Given labeled source image data and the unlabeled target one, PAGen operates in the frequency domain by decomposing images into content and style components, and learns to transfer target-domain styles to source images while preserving the original content and labels therein. Furthermore, unlike existing approaches that require auxiliary models or multi-stage training pipelines [4, 8, 12, 23, 29, 36], PAGen can be inserted (and removed in the inference phase) as a simple preprocessing module and trained end-to-end together with the downstream task in a single training stage, significantly simplifying the training process. Our main contributions can be summarized as follows:

- We introduce PAGen, a simple, efficient, yet effective UDA method that incorporates only a preprocessing module during training, which is fully discarded at inference to avoid any additional computational overhead.
- By inherently maintaining content consistency between style-adapted and source images, we propose a feature alignment loss to promote robust feature learning and boost performance.
- Comprehensive experiments on various DAOD benchmarks demonstrate the effectiveness of our approach, achieving consistently superior performance with improvements of 2.3% on Foggy Cityscapes, 3.1% on BDD100K Night, and an average of 1.7% on ACDC over state-of-the-art complicated methods.

2. Related works

We briefly review existing works on domain-adaptive object detection and domain robust learning in the frequency domain.

2.1. Domain-adaptive object detection

Early works on domain-adaptive object detection primarily rely on adversarial learning [15] to align feature distributions at both the image and object levels [5, 9, 21, 45, 49, 52, 60].

Another line of research models domain distributions with graph structures and reduces domain discrepancies via graph matching [33–35, 39, 40, 58]. For instance, DA-Faster [9] aligns feature distributions at both the image and object levels, while SIGMA [34] models source and target domains as graphs and performs domain adaptation via graph matching. However, due to the absence of ground-truth annotations in the target domain, the detector becomes biased toward the source domain and consequently exhibits limited performance on the target domain. To mitigate this issue, self-training methods have been proposed to leverage pseudo labels [4, 8, 12, 14, 27, 28, 36], generally following a mean-teacher framework [12, 50] with various data augmentations. For example, UMT [12] employs CycleGAN [59]-generated images to mitigate domain shifts. CMT [4] integrates mean-teacher with contrastive learning [19] to enhance the representative capability of pseudo labels. AT [36] combines adversarial domain learning with weak-strong augmentation. MTOR [3] employs mean-teacher to enforce region- and graph-level consistency. More recently, with the rise of VFMs, DT [29] utilizes DINOv2 [41] for offline pseudo-label generation and online feature distillation. SEEN-DA [32] employs semantic entropy to refine cross-domain features using CLIP’s textual encoder [43] and RegionCLIP’s visual encoder [57]. Despite their effectiveness, self-training methods often require multiple training stages and rely on threshold-based [12, 36] or complex pseudo-label selection criteria [8, 13], making them difficult to train and tune in practice.

2.2. Domain-robust learning in frequency domain

Images can be transformed into the frequency domain via various methods. For instance, the complex-valued discrete Fourier transform (DFT) [16] maps images into the frequency domain, which can be decomposed into phase and amplitude components, facilitating the style transfer of images by the manipulation of the amplitude spectrum. FDA [53] exploits this property and swaps the low-frequency bands of amplitude spectra between source and target images for domain-adaptive semantic segmentation. ARP [6] swaps the entire amplitude spectrum to enhance feature robustness. More recently, CISS [48] applies FDA to adapt between normal and adverse weather conditions for segmentation. Despite their efficiency in transferring style for DA, these methods rely on a fixed hyperparameter to determine which frequency bands are exchanged. This lack of adaptability across different domains or image instances prevents the model from fully realizing its performance potential. There also exist real-valued transformations, such as the discrete sine transform (DST) [17] and the discrete cosine transform (DCT) [1], which do not support phase-amplitude decomposition well. In these cases, the spectral signals are typically analyzed manually and partitioned into domain-invariant

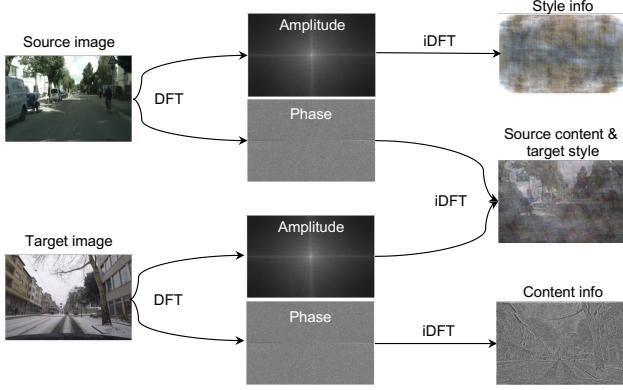


Figure 2. Image decomposition in the frequency domain allows separating content and style components for cross-image recombination.

and domain-variant frequency bands, which are then adapted separately in the latent frequency domain. This strategy is grounded in the observation that low-frequency components tend to be more domain-invariant and generalizable, while high-frequency components are often domain-specific and prone to overfitting [6, 37, 51]. For example, FSDR [24] and NightAdapter [2] leverage DCT and DST, respectively, to enhance domain-invariant features while attenuating domain-variant components for domain-generalizable semantic segmentation. However, because these methods rely on manual spectral analysis and handcrafted frequency partitioning, they are susceptible to human bias and result in suboptimal overall performance.

3. Proposed method

We start from reviewing the problem setup of UDA for object detection and the mechanism of image decomposition in the frequency domain for self-completeness. We then present the mechanism of our proposed PAGen and detail its integration into the DAOD task.

3.1. Preliminaries

UDA for object detection In the setting of UDA for object detection, we have a labeled source dataset $D^s = \{(x_i^s, b_i^s, c_i^s) \sim P(x^s, b^s, c^s)\}_{i=1}^{N_s}$, where x_i^s is the i -th of the N_s source images; b_i^s and c_i^s represent the corresponding labels of the bounding boxes and categories, respectively; s indicates the source dataset. We also have access to an unlabeled target data set $D^t = \{x_i^t \sim P(x^t)\}_{i=1}^{N_t}$, where x_i^t is the i -th of the target images N_t , and t indicates the target data set. In general, an object detector trained on D^s will have a performance drop when tested on D^t , especially if the domain gap between the two datasets is large. Here, we propose PAGen to reduce that gap.

Phase-amplitude decomposition of an image An image I of size $H \times W$ can be decomposed into phase and amplitude components after being transformed from the spatial to the frequency domain. Specifically, for each channel of the image, we can convert it from the real spatial domain to the complex frequency domain using the discrete Fourier transform (DFT):

$$\mathcal{F}(u, v) = \sum_{h, w} I(h, w) e^{-j2\pi(\frac{h}{H}u + \frac{w}{W}v)}, \quad (1)$$

where $j^2 = -1$ and (u, v) denotes the image coordinate. Then we can have the phase spectrum, the argument of \mathcal{F} at each frequency by:

$$\mathcal{F}^P(u, v) = \arctan\left(\frac{\text{Imag}(\mathcal{F}(u, v))}{\text{Real}(\mathcal{F}(u, v))}\right), \quad (2)$$

and amplitude spectrum, the absolute value of \mathcal{F} at each frequency by

$$\mathcal{F}^A(u, v) = \sqrt{\text{Real}(\mathcal{F}(u, v))^2 + \text{Imag}(\mathcal{F}(u, v))^2}, \quad (3)$$

where $\text{Real}(\cdot)$ and $\text{Imag}(\cdot)$ represent the real and imaginary parts of the complex \mathcal{F} , respectively. We use \mathcal{F}^{-1} to represent the discrete inverse Fourier transform (iDFT) that maps the spectrum back to the image domain. Perceptually, \mathcal{F}^P represents the content, while \mathcal{F}^A represents the style of an image, as illustrated in Fig. 2.

3.2. Phase-guided Amplitude Generation

As illustrated in Fig. 3(a), our proposed PAGen operates as a preprocessing module preceding the detection backbone. It is activated only during training, where it jointly processes paired source–target images. During inference, the PAGen module is entirely discarded, and target-domain images are directly fed into the detector. Specifically, We build PAGen upon a patch-based cross-attention framework, where the query is derived from the source phase, while the key and value are obtained from the source and target amplitudes, respectively. In this design, each style-free query patch, representing diverse object or background structures, learns to refine its style through the powerful global attention across both source and target amplitudes, narrowing the domain gap consequently.

As shown in Fig. 3(b), starting from two randomly paired input images I_s and I_t from the source and target datasets, respectively, we calculate the phase spectrum of the source image \mathcal{F}_s^P with Eq. 2, and the amplitude spectra \mathcal{F}_s^A and \mathcal{F}_t^A of both source and target images with Eq. 3, and use them as input to PAGen, as shown in Fig. 3(a). In the cross-attention framework, we use \mathcal{F}_s^P to generate the query Q :

$$Q = \text{DConv}^{3 \times 3}(\text{Conv}^{p \times p}(\mathcal{F}_s^P)), \quad (4)$$

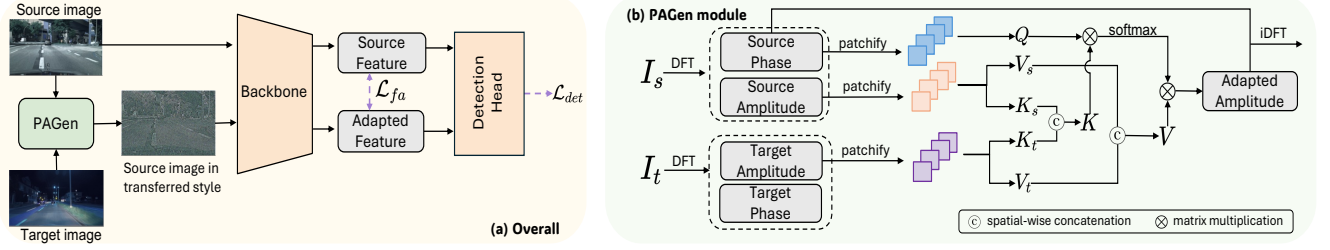


Figure 3. (a) Overview of our approach. The proposed PAGen is employed only during training as a preprocessing component for the detector. Given a source image and its style-altered PAGen output, we feed both into the detector and enforce feature alignment within the backbone’s latent space. This alignment is optimized jointly with the detector’s standard training objectives to learn the full pipeline. During inference time, PAGen is entirely discarded, and target-domain images are directly fed into the detector. (b) Architecture of PAGen. PAGen follows a patch-wise cross-attention paradigm. We transform source image I_s and target image I_t into frequency domain, use the source phase as the query branch, and construct key–value features by concatenating amplitude representations from both domains along the spatial dimension. Cross-attention yields an adapted amplitude, which is combined with the source phase and converted back via iDFT to produce the PAGen-adapted image.

in which \mathcal{F}_s^P is first patchified by a convolution operator $\text{Conv}^{p \times p}$ with both kernel size and stride of p (divisible by H and W), and simultaneously mapped to hidden dimension d_h . Then, a depthwise convolution [22] with kernel size 3 is used to project it to the query space. Similarly, we use \mathcal{F}_s^A and \mathcal{F}_t^A to generate keys K_s , K_t and values V_s , V_t from the source and target amplitude spectrum, respectively:

$$\begin{aligned} K_s &= \text{DConv}^{3 \times 3} (\text{Conv}^{p \times p} (\mathcal{F}_s^A)), \\ K_t &= \text{DConv}^{3 \times 3} (\text{Conv}^{p \times p} (\mathcal{F}_t^A)), \end{aligned} \quad (5)$$

$$\begin{aligned} V_s &= \text{DConv}^{3 \times 3} (\text{Conv}^{p \times p} (\mathcal{F}_s^A)), \\ V_t &= \text{DConv}^{3 \times 3} (\text{Conv}^{p \times p} (\mathcal{F}_t^A)). \end{aligned} \quad (6)$$

It is noteworthy that the convolution layers in Eqs. (4–6) are not shared. We then flatten the keys and values in the spatial dimensions and concatenate K_s and K_t , V_s and V_t pairwise in the flattened spatial dimension to formulate the key K and value V for the cross-attention framework:

$$K = \text{concat} (K_s, K_t), \quad (7)$$

$$V = \text{concat} (V_s, V_t). \quad (8)$$

We also flatten Q in Eq. (4) in the spatial dimensions and generate output amplitude A via the computation of the attention map [56]:

$$A = \text{Softmax} \left(\frac{QK^T}{t} \right) V, \quad (9)$$

in which t is a learnable temperature to scale the sharpness of the attention distribution. Here, we assume a single attention head for clarity, without loss of generality. We then reshape A back to separate spatial dimensions and generate the final output amplitude A^* :

$$A^* = \text{Conv}^{1 \times 1} (\text{Upsample} (A)), \quad (10)$$

in which Upsample is a bilinear interpolator that extends the size back to $H \times W$, and a point-wise convolution $\text{Conv}^{1 \times 1}$ is used to transform it back to the input channel C . Now we can get a style-transferred image whose content is consistent with the source image, by using iDFT to map \mathcal{F}_s^P and A^* back to image space:

$$I_a = \mathcal{F}^{-1} (\mathcal{F}_s^P, A^*), \quad (11)$$

in which I_a is the adapted image from the source domain to the target. It is used together with the source image I_s for model training to enhance feature robustness between source and target domains.

3.3. Feature alignment

To strengthen the consistency of learned features across the source and target domains, we additionally introduce a feature alignment loss, as illustrated in Fig. 3(a). This loss encourages alignment of the multi-stage backbone feature maps, facilitating the learning of domain-invariant representations:

$$\mathcal{L}_{fa} = \frac{1}{N} \sum_{i=1}^N \text{MSE} (F_i^s, F_i^a), \quad (12)$$

where the mean squared error MSE is computed between the source and adapted feature maps of the i^{th} stage of the backbone F_i^s , F_i^a , and averaged among all the N stages. In contrast to previous methods [9, 45] that align domains through adversarial learning at the distribution level, our approach directly adapts and aligns corresponding feature samples, achieving a more fine-grained and effective feature alignment.

3.4. PAGen in domain-adaptive object detection

We now describe how to incorporate PAGen into DAOD. PAGen is applied only during training as a preprocessing

Table 1. Domain adaptive object detection from Cityscapes to Foggy Cityscapes. The best performances are in **bold**, and the second-best are underlined. The corresponding technical properties of each method are listed as: Alignment (adversarial domain alignment and graph matching), Self-training (online pseudo-label generation or self-distillation), and VFM-based (offline pseudo-label generation, feature distillation, or fine-tuning).

Method	Technical properties			Person	Rider	Car	Truck	Bus	Train	Motor	Bicycle	mAP
	Alignment	Self-training	VFM-based									
DA-Faster [9]	✓			29.2	40.4	43.4	19.7	38.3	28.5	23.7	32.7	32.0
DICN [25]	✓			47.3	57.4	64.0	22.7	45.6	29.6	38.6	47.4	44.1
NLTE [39]	✓			43.1	50.7	58.7	33.6	56.7	42.7	33.7	43.3	45.4
PT [8]		✓		43.2	52.4	63.4	33.4	56.6	37.8	41.3	48.7	47.1
CMT [4]		✓		47.0	55.7	64.5	39.4	63.2	51.9	40.3	53.1	51.9
MIC [23]	✓	✓		50.9	55.3	67.0	33.9	52.4	33.7	40.6	47.5	47.6
AT [36]	✓	✓		45.5	55.1	64.2	35.0	56.3	<u>54.3</u>	38.5	51.9	50.9
DSD-DA [14]	✓	✓		49.0	59.6	65.3	35.7	61.0	46.5	43.9	57.3	52.3
CAT [28]	✓	✓		44.6	57.1	63.7	40.8	<u>66.0</u>	49.7	44.9	53.0	52.5
NSA-UDA [58]	✓	✓		50.3	60.1	67.7	37.4	57.4	46.9	47.3	54.3	52.7
REACT [31]	✓	✓		51.4	57.9	67.4	37.7	58.4	52.8	44.6	54.6	53.1
DT [29]		✓	✓	48.5	60.0	65.4	47.2	66.5	52.9	46.2	56.7	55.4
DA-Pro [30]	✓	✓	✓	55.4	62.9	70.9	40.3	63.4	54.0	42.3	58.0	55.9
SEEN-DA [32]	✓	✓	✓	58.5	64.5	71.7	42.0	61.2	54.8	47.1	59.9	<u>57.5</u>
PAGen (Ours)				63.7	65.5	74.3	<u>46.1</u>	63.9	49.9	50.8	64.3	59.8

module and is discarded at inference, ensuring zero additional computational overhead.

PAGen as a pre-processing module As illustrated in Fig. 3(b), given one source-domain image and a target-domain counterpart, PAGen generates the adapted image, which is fed into the backbone alongside the original source image. Since the adapted image preserves the content of the source image, the source ground-truth annotations can be directly used to supervise the adapted image. Accordingly, the object detection loss for both the source and adapted images can be expressed as (without loss of generality, we here adopt Faster R-CNN [44] for illustration):

$$\mathcal{L}_{det} = \mathcal{L}_s^{rpn} + \mathcal{L}_s^{roi} + \mathcal{L}_a^{rpn} + \mathcal{L}_a^{roi}, \quad (13)$$

where \mathcal{L}_s^{rpn} , \mathcal{L}_a^{rpn} , \mathcal{L}_s^{roi} , and \mathcal{L}_a^{roi} denote the region proposal loss from the region proposal network, and box regression and classification loss from the region-of-interest layer, on the source and adapted images, respectively. We find that these losses have similar ranges and do not need to be weighted against each other. With the style adaptation at the input level, the model can learn robust and transferable features for testing in the target domain.

Overall optimization objective Combining the object detection loss of Eq. 13 and the feature alignment loss of Eq. 12 leads to our overall optimization objective in the form of

$$\mathcal{L}_{PAGen} = \mathcal{L}_{det} + \lambda \mathcal{L}_{fa}, \quad (14)$$

where λ helps to balance the two losses.

4. Experiments

We extensively compare our proposal with state-of-the-art methods on various datasets and present comprehensive ablation studies.

4.1. Datasets

We employ five popularly used dataset for comparison:

- **ACDC** [47] is a real-world autonomous driving dataset covering four adverse weather conditions: fog, night, rain, and snow. Its object detection annotations are consistent with Cityscapes [10]. Each weather condition includes 400 training images and 100 validation images (except for night, which has 106 validation images). Following prior work [29], we train and evaluate our models separately on each of the four weather splits.
- **Cityscapes** [10] is a real-world autonomous driving dataset comprising 2,975 training images and 500 validation images for 8 classes.
- **Foggy Cityscapes** [46] is a synthetic dataset derived from Cityscapes that simulates fog at three intensity levels (0.005, 0.01, 0.02). Its annotations are inherited from Cityscapes. The dataset contains 8,925 images for training and 1,500 for validation. Following prior work [29, 32], we use the full dataset in our experiments.
- **BDD100K** [55] is a real-world autonomous driving dataset with annotations for 10 classes. Following prior works [27], we use the day and night training splits, which

contain 36,728 and 27,971 images, respectively, and the night validation split, which contains 3,929 images.

- **Sim10k** [26] is a synthetic dataset generated from the GTA V game¹. It contains 10,000 images with the class *car* for object detection labels.

4.2. Implementation details

We implement our method based on MMDetection [7]. We adopt ResNet50 [18] pre-trained on COCO [38] as the backbone and use Faster R-CNN [44] as the detection framework. In general, we follow the default training configurations in MMDetection, except that we set the batch size to 2 to include one source image and one target image per iteration. All experiments are conducted on an H100 GPU.

For the hyper-parameters in PAGen, we set the patch size to 16 and resize input images such that their spatial dimensions are divisible by this patch size. We set the number of heads to 4, the number of hidden dimensions to 32, and the loss weight λ in Eq. 14 to 1.

4.3. Results and comparisons

We employ the mean average precision (mAP) with a threshold of 0.5 as the evaluation metric. All experimental setups are listed below:

- **Cityscapes** \rightarrow **Foggy Cityscapes** measures adaptation from real-world clear weather to synthetic foggy conditions. As shown in Table 1, PAGen surpasses all compared methods in terms of mAP, improving the state-of-the-art from 57.5% to 59.8% (+2.3%). In particular, our method outperforms 5 of the 8 categories (person, rider, car, motor, and bicycle), with gains ranging from 1% to 5.2%.
- **Sim10k** \rightarrow **Cityscapes** assesses adaptation from synthetic images generated by the GTA V game engine to real-world driving scenes. As shown in Table 2, PAGen improves the state-of-the-art performance to 69.9% mAP, achieving a gain of 3.1%.
- **BDD100K Day** \rightarrow **Night** evaluates adaptation from real-world daytime to nighttime driving scenes. As shown in Table 3, PAGen achieves the best performance of 49.5%, improving upon the current state-of-the-art method by 3.1%. Following prior work, we exclude the *train* class from evaluation due to its limited annotations. Notably, our method outperforms 7 out of the 9 evaluated classes, with performance gains ranging from 2.2% to 8.9%.
- **Cityscapes** \rightarrow **ACDC** evaluates adaptation from real-world normal weather to adverse weather conditions. As shown in Table 4, PAGen achieves performance improvements in 3 out of the 4 adverse weather settings, with gains ranging from 1.2% to 4.6%. On average, PAGen improves performance by 1.7% across all four conditions.

¹Rockstar Games, Grand Theft Auto V, Rockstar North, 2013.

Table 2. Domain adaptive object detection from Sim10k to Cityscapes.

Method	Technical properties			mAP
	Alignment	Self-training	VFM-based	
LRA [42]	✓			55.7
DA-Faster [9]	✓			38.2
SCAN [33]	✓			52.6
CIGAR [40]	✓			58.5
OADA [54]	✓			59.2
DSD-DA [14]	✓	✓		52.5
NSA-UDA [58]	✓	✓		56.3
SIGMA++ [35]	✓	✓		57.7
REACT [31]	✓	✓		58.6
SOCCER [11]	✓	✓		63.8
DA-Pro [30]	✓	✓	✓	62.9
SEEN-DA [32]	✓	✓	✓	<u>66.8</u>
PAGen (Ours)				69.9

4.4. Ablation Studies

To validate the effectiveness of the proposed method, we conduct ablation studies on the challenging Cityscapes \rightarrow ACDC benchmark, which involves adaptation from clear-weather images to images under various adverse conditions in the real-world scenario.

Learning-based vs. Human-Tuned Amplitude Generation Starting from the original FDA [53], we progressively evaluate the contributions of the proposed PAGen architecture. Following FDA, we substitute the source amplitude with the target amplitude using $\beta \in \{0.01, 0.05, 0.09\}$. For the design of the cross-attention (CA) module, we first test using only the target amplitude, and then using both source and target amplitudes to generate the key-value pairs. As shown in Table 5, vanilla FDA exhibits variable performance as β increases, ranging from a -3.1% drop (*Snow*) to a $+4.4\%$ gain (*Rain*). This indicates that tuning β is necessary to optimize spectral manipulation under different real-world adverse conditions.

On the other hand, our proposed PAGen outperforms FDA by leveraging the global patch-wise reference of the cross-attention module to learn and generate spectra for domain adaptation. As shown in Table 5, using only the target amplitude in PAGen yields performance comparable to FDA, indicating that incorporating the source amplitude is essential for producing an optimal spectrum, which is consistent with the original motivation of FDA. When introducing the source amplitude, applying cross-attention PAGen yields the best performance and consistently surpasses FDA across all four splits, from 0.3% on *Rain* to 3.0% on *Fog*. These results demonstrate the superiority of leveraging global reference information from both source and target amplitudes simultaneously when predicting the attention map. A qualitative

Table 3. Results of domain adaptive object detection from BDD100K Day to Night.

Method	Technical properties		Pedestrian	Rider	Car	Truck	Bus	Motor cycle	Bicycle	Traffic Light	Traffic Sign	mAP
	Alignment	Self-training										
DA-Faster [9]	✓		50.4	30.3	66.3	46.8	48.3	32.6	41.4	41.0	56.2	41.3
TDD [20]		✓	43.1	20.7	68.4	33.3	35.6	16.5	25.9	43.1	59.5	34.6
UMT [12]		✓	46.5	26.1	46.8	44.0	46.3	28.2	40.2	31.6	52.7	36.2
2PCNet [27]		✓	<u>54.4</u>	<u>30.8</u>	<u>73.1</u>	53.8	55.2	<u>37.5</u>	<u>44.5</u>	<u>49.4</u>	<u>65.2</u>	<u>46.4</u>
AT [36]	✓	✓	42.3	30.4	60.8	48.9	<u>52.1</u>	34.5	42.7	29.1	43.9	38.5
PAGen (Ours)			61.0	39.7	75.3	<u>49.7</u>	48.9	45.3	48.4	57.0	70.1	49.5

Table 4. Domain adaptive object detection from Cityscapes to ACDC on the four weather splits.

Method	Technical properties			Fog	Night	Rain	Snow
	Alignment	Self-training	VFM-based				
AT [36]	✓	✓		62.2	29.5	37.7	55.2
DT [29]		✓	✓	68.6	<u>36.4</u>	<u>39.0</u>	<u>56.8</u>
PAGen (Ours)				<u>67.8</u>	37.6	43.6	58.6

Table 5. Ablation study w.r.t. model architectures by domain adaption from Cityscapes to ACDC.

Method	Settings		Fog	Night	Rain	Snow
	Source amp.	Target amp.				
FDA [53] ($\beta = 0.01$)	✓	✓	<u>64.8</u>	<u>36.0</u>	38.9	56.8
FDA [53] ($\beta = 0.05$)	✓	✓	62.7	34.8	41.7	54.0
FDA [53] ($\beta = 0.09$)	✓	✓	63.0	34.2	<u>43.3</u>	53.7
PAGen (Ours)		✓	63.3	35.1	41.8	<u>57.1</u>
PAGen (Ours)	✓	✓	67.8	37.6	43.6	58.6

Table 6. Ablation study w.r.t. different λ values for the feature alignment loss by domain adaption from Cityscapes to ACDC.

	$\lambda = 0$	$\lambda = 0.1$	$\lambda = 0.5$	$\lambda = 1$	$\lambda = 5$
Fog	65.3	<u>67.2</u>	65.8	67.8	65.3
Night	35.2	35.5	37.7	<u>37.6</u>	35.8
Rain	41.9	<u>42.2</u>	41.8	43.6	40.2
Snow	56.0	56.5	57.8	58.6	<u>58.3</u>

comparison between FDA ($\beta = 0.01$) and PAGen on the Cityscapes to ACDC setup across all four adverse conditions is presented in Fig. 4.

λ in the Feature Alignment loss We analyze the effect of varying λ values in Eq. 14. As presented in Table 6, setting $\lambda = 1$ yields the highest performance, with an average

Table 7. Ablation studies w.r.t. the number of attention heads by domain adaption from Cityscapes to ACDC.

# Attention heads	Fog	Night	Rain	Snow
8	66.2	34.4	42.0	59.0
4	67.8	37.6	43.6	<u>58.6</u>
2	<u>67.3</u>	<u>37.1</u>	<u>43.0</u>	58.0

Table 8. Ablation studies of domain adaptive object detection from Cityscapes to ACDC on the patch sizes.

Patch size	Fog	Night	Rain	Snow
64	<u>66.6</u>	<u>37.0</u>	<u>42.9</u>	<u>57.5</u>
32	64.0	36.3	41.9	56.5
16	67.8	37.6	43.6	58.6

improvement of 2.3%. Furthermore, all tested λ values consistently improve performance over the no-alignment case, emphasizing the crucial role of feature alignment in PAGen.

Number of attention heads We investigate the impact of the number of attention heads on the performance of PAGen. As shown in Table 7, the overall performance generally improves and saturates as the number of attention heads increases from 2 to 4, with the exception of the *Snow* condition. While *Snow* sees an additional 0.4% gain when the number of heads increases from 4 to 8, the performance on the other three splits decreases, ranging from 1.6% (*Fog* and *Rain*) to 3.2% (*Night*). Although varying the number of attention heads triggers slight performance fluctuations, all configurations can achieve comparable or superior performance than the peer methods presented in Table 4, demonstrating the effectiveness of our approach.

Influence of patch size We examine the effect of patch size on PAGen’s performance. As shown in Table 8, performance initially decreases when the patch size is reduced



Figure 4. Examples of detection results on each weather split of the ACDC dataset.

Table 9. Ablation studies of domain adaptive object detection from Cityscapes to ACDC on the number of hidden dimensions.

# Hidden dimensions	Fog	Night	Rain	Snow
64	<u>67.3</u>	33.2	42.4	<u>58.1</u>
32	67.8	37.6	43.6	58.6
16	65.5	<u>34.2</u>	<u>42.7</u>	57.8

from 64 to 32, but then improves when the patch size is further reduced to 16. This result indicates a non-monotonic relationship between model performance and patch size granularity, which we attribute to the trade-off between learning global and local information during training.

Number of hidden dimensions We investigate the impact of varying the number of hidden dimensions on PAGen’s performance. As shown in Table 9, all four splits achieve the highest performance when the number of hidden dimensions is set to 32. Reducing the hidden dimensions to 16 or increasing them to 64 leads to performance drops ranging from 0.5% (*Fog* and *Snow*) to 4.4% (*Night*), likely due to underfitting or overfitting.

Domain alignment visualization We take Cityscapes and ACDC (*Snow*) as an example to illustrate the domain alignment effect. As shown in Fig. 5, although also working in the frequency domain, FDA produces feature embeddings of the two datasets that are clearly separated. In contrast, those extracted by PAGen are almost completely overlapped, indicating a stronger robustness against domain difference. This observation exhibits the effectiveness of learning-based design in transferring target-domain styles to source images,

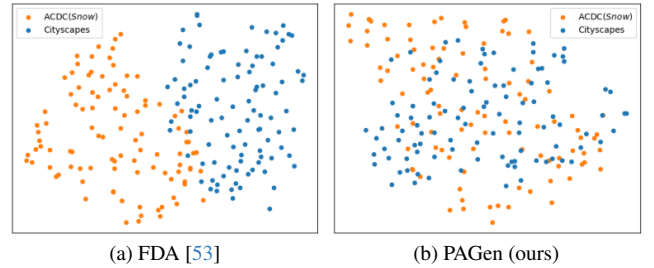


Figure 5. t-SNE visualization of embedding features from ACDC (*Snow*) and Cityscapes, illustrating their domain discrepancy and the representational structure learned by the model.

leading to the superior performance of PAGen.

5. Conclusion

We introduce PAGen, a simple, efficient, yet effective learnable preprocessing module that facilitates unsupervised domain adaptive object detection. Operating in the frequency space, PAGen preserves content-related components from the labeled source domain while adapting style-related components across source and target domains, thereby enhancing the robustness of detectors under domain shifts. Evaluations on multiple DAOD benchmarks demonstrate the superior performance of PAGen over existing approaches.

The main limitation of PAGen lies in addressing content-triggered domain gaps. This is primarily because PAGen relies solely on the phase information from the source domain and does not incorporate phase cues from the target domain. As future work, we plan to investigate phase information fusion to better adapt content-level discrepancies across domains.

References

- [1] N. Ahmed, T. Natarajan, and K.R. Rao. Discrete cosine transform. *IEEE Transactions on Computers*, C-23(1):90–93, 1974. 2
- [2] Qi Bi, Jingjun Yi, Huimin Huang, Hao Zheng, Haolan Zhan, Yawen Huang, Yuexiang Li, Xian Wu, and Yefeng Zheng. Nightadapter: Learning a frequency adapter for generalizable night-time scene segmentation. In *Proceedings of the IEEE/CVF Conference on Computer Vision and Pattern Recognition (CVPR)*, pages 23838–23849, 2025. 3
- [3] Qi Cai, Yingwei Pan, Chong-Wah Ngo, Xinmei Tian, Lingyu Duan, and Ting Yao. Exploring object relation in mean teacher for cross-domain detection. In *2019 IEEE/CVF Conference on Computer Vision and Pattern Recognition (CVPR)*, pages 11449–11458, 2019. 2
- [4] Shengcao Cao, Dhiraj Joshi, Liang-Yan Gui, and Yu-Xiong Wang. Contrastive mean teacher for domain adaptive object detectors. In *2023 IEEE/CVF Conference on Computer Vision and Pattern Recognition (CVPR)*, pages 23839–23848, 2023. 1, 2, 5
- [5] Chaoqi Chen, Zebiao Zheng, Xinghao Ding, Yue Huang, and Qi Dou. Harmonizing transferability and discriminability for adapting object detectors. In *Proceedings of the IEEE/CVF Conference on Computer Vision and Pattern Recognition (CVPR)*, 2020. 1, 2
- [6] Guangyao Chen, Peixi Peng, Li Ma, Jia Li, Lin Du, and Yonghong Tian. Amplitude-phase recombination: Rethinking robustness of convolutional neural networks in frequency domain. In *Proceedings of the IEEE/CVF International Conference on Computer Vision (ICCV)*, pages 458–467, 2021. 2, 3
- [7] Kai Chen, Jiaqi Wang, Jiangmiao Pang, Yuhang Cao, Yu Xiong, Xiaoxiao Li, Shuyang Sun, Wansen Feng, Ziwei Liu, Jiarui Xu, Zheng Zhang, Dazhi Cheng, Chenchen Zhu, Tianheng Cheng, Qijie Zhao, Buyu Li, Xin Lu, Rui Zhu, Yue Wu, Jifeng Dai, Jingdong Wang, Jianping Shi, Wanli Ouyang, Chen Change Loy, and Dahua Lin. MMDetection: Open mmlab detection toolbox and benchmark. *arXiv preprint arXiv:1906.07155*, 2019. 6
- [8] Meilin Chen, Weijie Chen, Shicai Yang, Jie Song, Xinchao Wang, Lei Zhang, Yunfeng Yan, Donglian Qi, Yueting Zhuang, Di Xie, and Shiliang Pu. Learning domain adaptive object detection with probabilistic teacher. In *Proceedings of the 39th International Conference on Machine Learning*, pages 3040–3055. PMLR, 2022. 1, 2, 5
- [9] Yuhua Chen, Wen Li, Christos Sakaridis, Dengxin Dai, and Luc Van Gool. Domain adaptive faster r-cnn for object detection in the wild. In *Proceedings of the IEEE Conference on Computer Vision and Pattern Recognition (CVPR)*, 2018. 1, 2, 4, 5, 6, 7
- [10] Marius Cordts, Mohamed Omran, Sebastian Ramos, Timo Rehfeld, Markus Enzweiler, Rodrigo Benenson, Uwe Franke, Stefan Roth, and Bernt Schiele. The cityscapes dataset for semantic urban scene understanding. In *2016 IEEE Conference on Computer Vision and Pattern Recognition (CVPR)*, pages 3213–3223, 2016. 5
- [11] Yiming Cui, Liang Li, Jiehua Zhang, Chenggang Yan, Hongkui Wang, Shuai Wang, Jin Heng, and Wu Li. Stochastic context consistency reasoning for domain adaptive object detection. In *ACM Multimedia 2024*, 2024. 6
- [12] Jinhong Deng, Wen Li, Yuhua Chen, and Lixin Duan. Unbiased mean teacher for cross-domain object detection. In *Proceedings of the IEEE/CVF Conference on Computer Vision and Pattern Recognition (CVPR)*, pages 4091–4101, 2021. 1, 2, 7
- [13] Jinhong Deng, Dongli Xu, Wen Li, and Lixin Duan. Harmonious teacher for cross-domain object detection. In *Proceedings of the IEEE/CVF Conference on Computer Vision and Pattern Recognition (CVPR)*, pages 23829–23838, 2023. 2
- [14] Yongchao Feng, Shiwei Li, Yingjie Gao, Ziyue Huang, Yanan Zhang, Qingjie Liu, and Yunhong Wang. DSD-DA: Distillation-based source debiasing for domain adaptive object detection. In *Proceedings of the 41st International Conference on Machine Learning*, pages 13225–13240. PMLR, 2024. 1, 2, 5, 6
- [15] Yaroslav Ganin and Victor Lempitsky. Unsupervised domain adaptation by backpropagation. In *Proceedings of the 32nd International Conference on Machine Learning*, pages 1180–1189, Lille, France, 2015. PMLR. 2
- [16] Rafael C. Gonzalez and Richard E. Woods. *Digital image processing*. Pearson, New York, NY, 2018. 2
- [17] A. Gupta and K.R. Rao. A fast recursive algorithm for the discrete sine transform. *IEEE Transactions on Acoustics, Speech, and Signal Processing*, 38(3):553–557, 1990. 2
- [18] Kaiming He, Xiangyu Zhang, Shaoqing Ren, and Jian Sun. Deep residual learning for image recognition. In *Proceedings of the IEEE Conference on Computer Vision and Pattern Recognition (CVPR)*, 2016. 6
- [19] Kaiming He, Haoqi Fan, Yuxin Wu, Saining Xie, and Ross Girshick. Momentum contrast for unsupervised visual representation learning. In *Proceedings of the IEEE/CVF Conference on Computer Vision and Pattern Recognition (CVPR)*, 2020. 2
- [20] Mengzhe He, Yali Wang, Jiayi Wu, Yiru Wang, Hanqing Li, Bo Li, Weihao Gan, Wei Wu, and Yu Qiao. Cross domain object detection by target-perceived dual branch distillation. In *Proceedings of the IEEE/CVF Conference on Computer Vision and Pattern Recognition (CVPR)*, pages 9570–9580, 2022. 7
- [21] Zhenwei He and Lei Zhang. Multi-adversarial faster-rcnn for unrestricted object detection. In *Proceedings of the IEEE/CVF International Conference on Computer Vision (ICCV)*, 2019. 1, 2
- [22] Andrew G. Howard, Menglong Zhu, Bo Chen, Dmitry Kalenichenko, Weijun Wang, Tobias Weyand, Marco Andreetto, and Hartwig Adam. Mobilenets: Efficient convolutional neural networks for mobile vision applications. *ArXiv*, abs/1704.04861, 2017. 4
- [23] Lukas Hoyer, Dengxin Dai, Haoran Wang, and Luc Van Gool. Mic: Masked image consistency for context-enhanced domain adaptation. In *2023 IEEE/CVF Conference on Computer Vision and Pattern Recognition (CVPR)*, pages 11721–11732, 2023. 2, 5

- [24] Jiaxing Huang, Dayan Guan, Aoran Xiao, and Shijian Lu. Fsdrr: Frequency space domain randomization for domain generalization. In *Proceedings of the IEEE/CVF Conference on Computer Vision and Pattern Recognition (CVPR)*, pages 6891–6902, 2021. 3
- [25] Yifan Jiao, Hantao Yao, and Changsheng Xu. Dual instance-consistent network for cross-domain object detection. *IEEE Transactions on Pattern Analysis and Machine Intelligence*, 45(6):7338–7352, 2023. 5
- [26] Matthew Johnson-Roberson, Charlie Barto, Rounak Mehta, Sharath Nittur Sridhar, Karl Rosaen, and Ram Vasudevan. Driving in the matrix: Can virtual worlds replace human-generated annotations for real world tasks? *2017 IEEE International Conference on Robotics and Automation (ICRA)*, pages 746–753, 2016. 6
- [27] Mikhail Kennerley, Jian-Gang Wang, Bharadwaj Veeravalli, and Robby T. Tan. 2pcnet: Two-phase consistency training for day-to-night unsupervised domain adaptive object detection. In *Proceedings of the IEEE/CVF Conference on Computer Vision and Pattern Recognition (CVPR)*, pages 11484–11493, 2023. 1, 2, 5, 7
- [28] Mikhail Kennerley, Jian-Gang Wang, Bharadwaj Veeravalli, and Robby T. Tan. Cat: Exploiting inter-class dynamics for domain adaptive object detection. In *2024 IEEE/CVF Conference on Computer Vision and Pattern Recognition (CVPR)*, pages 16541–16550, 2024. 1, 2, 5
- [29] Marc-Antoine Lavoie, Anas Mahmoud, and Steven L. Waslander. Large self-supervised models bridge the gap in domain adaptive object detection. In *Proceedings of the IEEE/CVF Conference on Computer Vision and Pattern Recognition (CVPR)*, pages 4692–4702, 2025. 1, 2, 5, 7
- [30] Haochen Li, Rui Zhang, Hantao Yao, Xinkai Song, Yifan Hao, Yongwei Zhao, Ling Li, and Yunji Chen. Learning domain-aware detection head with prompt tuning. In *Advances in Neural Information Processing Systems*, pages 4248–4262. Curran Associates, Inc., 2023. 1, 5, 6
- [31] Haochen Li, Rui Zhang, Hantao Yao, Xin Zhang, Yifan Hao, Xinkai Song, and Ling Li. React: Remainder adaptive compensation for domain adaptive object detection. *IEEE Transactions on Image Processing*, 33:3735–3748, 2024. 5, 6
- [32] Haochen Li, Rui Zhang, Hantao Yao, Xin Zhang, Yifan Hao, Xinkai Song, Shaohui Peng, Yongwei Zhao, Chen Zhao, Yanjun Wu, and Ling Li. Seen-da: Semantic entropy guided domain-aware attention for domain adaptive object detection. In *Proceedings of the IEEE/CVF Conference on Computer Vision and Pattern Recognition (CVPR)*, pages 25465–25475, 2025. 1, 2, 5, 6
- [33] Wuyang Li, Xinyu Liu, Xiwen Yao, and Yixuan Yuan. Scan: Cross domain object detection with semantic conditioned adaptation. *Proceedings of the AAAI Conference on Artificial Intelligence*, 36(2):1421–1428, 2022. 1, 2, 6
- [34] Wuyang Li, Xinyu Liu, and Yixuan Yuan. Sigma: Semantic-complete graph matching for domain adaptive object detection. In *Proceedings of the IEEE/CVF Conference on Computer Vision and Pattern Recognition (CVPR)*, pages 5291–5300, 2022. 2
- [35] Wuyang Li, Xinyu Liu, and Yixuan Yuan. Sigma++: Improved semantic-complete graph matching for domain adaptive object detection. *IEEE Transactions on Pattern Analysis and Machine Intelligence*, 45(7):9022–9040, 2023. 1, 2, 6
- [36] Yu-Jhe Li, Xiaoliang Dai, Chih-Yao Ma, Yen-Cheng Liu, Kan Chen, Bichen Wu, Zijian He, Kris Kitani, and Peter Vajda. Cross-domain adaptive teacher for object detection. In *IEEE Conference on Computer Vision and Pattern Recognition (CVPR)*, 2022. 1, 2, 5, 7
- [37] Shiqi Lin, Zhizheng Zhang, Zhipeng Huang, Yan Lu, Cuiling Lan, Peng Chu, Quanzeng You, Jiang Wang, Zicheng Liu, Amey Parulkar, Viraj Navkal, and Zhibo Chen. Deep frequency filtering for domain generalization. In *Proceedings of the IEEE/CVF Conference on Computer Vision and Pattern Recognition (CVPR)*, pages 11797–11807, 2023. 3
- [38] Tsung-Yi Lin, Michael Maire, Serge J. Belongie, James Hays, Pietro Perona, Deva Ramanan, Piotr Dollár, and C. Lawrence Zitnick. Microsoft coco: Common objects in context. In *European Conference on Computer Vision*, 2014. 6
- [39] Xinyu Liu, Wuyang Li, Qiushi Yang, Baopu Li, and Yixuan Yuan. Towards robust adaptive object detection under noisy annotations. In *Proceedings of the IEEE/CVF Conference on Computer Vision and Pattern Recognition (CVPR)*, pages 14207–14216, 2022. 1, 2, 5
- [40] Yabo Liu, Jinghua Wang, Chao Huang, Yaowei Wang, and Yong Xu. Cigar: Cross-modality graph reasoning for domain adaptive object detection. In *2023 IEEE/CVF Conference on Computer Vision and Pattern Recognition (CVPR)*, pages 23776–23786, 2023. 1, 2, 6
- [41] Maxime Oquab, Timothée Darcet, Théo Moutakanni, Huy V. Vo, Marc Szafraniec, Vasil Khalidov, Pierre Fernandez, Daniel HAZIZA, Francisco Massa, Alaaeldin El-Nouby, Mido Assran, Nicolas Ballas, Wojciech Galuba, Russell Howes, Po-Yao Huang, Shang-Wen Li, Ishan Misra, Michael Rabbat, Vasu Sharma, Gabriel Synnaeve, Hu Xu, Herve Jegou, Julien Mairal, Patrick Labatut, Armand Joulin, and Piotr Bojanowski. DINOv2: Learning robust visual features without supervision. *Transactions on Machine Learning Research*, 2024. Featured Certification. 2
- [42] Zhengquan Piao, Linbo Tang, and Baojun Zhao. Unsupervised domain-adaptive object detection via localization regression alignment. *IEEE Transactions on Neural Networks and Learning Systems*, 35(11):15170–15181, 2024. 6
- [43] Alec Radford, Jong Wook Kim, Chris Hallacy, Aditya Ramesh, Gabriel Goh, Sandhini Agarwal, Girish Sastry, Amanda Askell, Pamela Mishkin, Jack Clark, Gretchen Krueger, and Ilya Sutskever. Learning transferable visual models from natural language supervision. In *Proceedings of the 38th International Conference on Machine Learning (ICML)*, pages 8748–8763. PMLR, 2021. 2
- [44] Shaoqing Ren, Kaiming He, Ross Girshick, and Jian Sun. Faster r-cnn: Towards real-time object detection with region proposal networks. In *Advances in Neural Information Processing Systems*. Curran Associates, Inc., 2015. 5, 6
- [45] Kuniaki Saito, Yoshitaka Ushiku, Tatsuya Harada, and Kate Saenko. Strong-weak distribution alignment for adaptive object detection. In *Proceedings of the IEEE/CVF Conference on Computer Vision and Pattern Recognition (CVPR)*, 2019. 1, 2, 4

- [46] Christos Sakaridis, Dengxin Dai, and Luc Van Gool. Semantic foggy scene understanding with synthetic data. *International Journal of Computer Vision*, 126:973 – 992, 2017. [5](#)
- [47] Christos Sakaridis, Dengxin Dai, and Luc Van Gool. Acdc: The adverse conditions dataset with correspondences for semantic driving scene understanding. In *Proceedings of the IEEE/CVF International Conference on Computer Vision (ICCV)*, pages 10765–10775, 2021. [5](#)
- [48] Christos Sakaridis, David Bruggemann, Fisher Yu, and Luc Van Gool. Condition-invariant semantic segmentation. *IEEE Transactions on Pattern Analysis and Machine Intelligence*, 47(4):3111–3125, 2025. [2](#)
- [49] Peng Su, Kun Wang, Xingyu Zeng, Shixiang Tang, Dapeng Chen, Di Qiu, and Xiaogang Wang. Adapting object detectors with conditional domain normalization. In *Proceedings of the European Conference on Computer Vision (ECCV)*, pages 403–419. Springer, 2020. [1](#), [2](#)
- [50] Antti Tarvainen and Harri Valpola. Mean teachers are better role models: Weight-averaged consistency targets improve semi-supervised deep learning results. In *Advances in Neural Information Processing Systems*. Curran Associates, Inc., 2017. [1](#), [2](#)
- [51] Haohan Wang, Xindi Wu, Zeyi Huang, and Eric P. Xing. High-frequency component helps explain the generalization of convolutional neural networks. In *Proceedings of the IEEE/CVF Conference on Computer Vision and Pattern Recognition (CVPR)*, 2020. [3](#)
- [52] Chang-Dong Xu, Xing-Ran Zhao, Xin Jin, and Xiu-Shen Wei. Exploring categorical regularization for domain adaptive object detection. In *Proceedings of the IEEE/CVF Conference on Computer Vision and Pattern Recognition (CVPR)*, 2020. [1](#), [2](#)
- [53] Yanchao Yang and Stefano Soatto. Fda: Fourier domain adaptation for semantic segmentation. In *Proceedings of the IEEE/CVF Conference on Computer Vision and Pattern Recognition (CVPR)*, 2020. [2](#), [6](#), [7](#), [8](#)
- [54] Jayeon Yoo, Inseop Chung, and Nojun Kwak. Unsupervised domain adaptation for one-stage object detector using offsets to bounding box. In *Computer Vision – ECCV 2022*, pages 691–708, Cham, 2022. Springer Nature Switzerland. [6](#)
- [55] Fisher Yu, Haofeng Chen, Xin Wang, Wenqi Xian, Yingying Chen, Fangchen Liu, Vashisht Madhavan, and Trevor Darrell. Bdd100k: A diverse driving dataset for heterogeneous multi-task learning. In *2020 IEEE/CVF Conference on Computer Vision and Pattern Recognition (CVPR)*, pages 2633–2642, 2020. [5](#)
- [56] Syed Waqas Zamir, Aditya Arora, Salman Khan, Munawar Hayat, Fahad Shahbaz Khan, and Ming-Hsuan Yang. Restormer: Efficient transformer for high-resolution image restoration. In *Proceedings of the IEEE/CVF Conference on Computer Vision and Pattern Recognition (CVPR)*, pages 5728–5739, 2022. [4](#)
- [57] Yiwu Zhong, Jianwei Yang, Pengchuan Zhang, Chunyuan Li, Noel Codella, Liunian Harold Li, Luowei Zhou, Xiyang Dai, Lu Yuan, Yin Li, and Jianfeng Gao. Regionclip: Region-based language-image pretraining. In *Proceedings of the IEEE/CVF Conference on Computer Vision and Pattern Recognition (CVPR)*, pages 16793–16803, 2022. [2](#)
- [58] Wenzhang Zhou, Heng Fan, Tiejian Luo, and Libo Zhang. Unsupervised domain adaptive detection with network stability analysis. In *2023 IEEE/CVF International Conference on Computer Vision (ICCV)*, pages 6963–6972, 2023. [1](#), [2](#), [5](#), [6](#)
- [59] Jun-Yan Zhu, Taesung Park, Phillip Isola, and Alexei A Efros. Unpaired image-to-image translation using cycle-consistent adversarial networks. In *Computer Vision (ICCV), 2017 IEEE International Conference on*, 2017. [2](#)
- [60] Xinge Zhu, Jiangmiao Pang, Ceyuan Yang, Jianping Shi, and Dahua Lin. Adapting object detectors via selective cross-domain alignment. In *Proceedings of the IEEE/CVF Conference on Computer Vision and Pattern Recognition (CVPR)*, 2019. [1](#), [2](#)